Three-dimensional simulation of stratospheric background aerosol: First results of a multiannual general circulation model simulation

Claudia Timmreck

Max-Planck-Institut für Meteorologie, Hamburg, Germany

Abstract. A sulfuric acid aerosol model has been implemented in the global general circulation model ECHAM4. This model treats the formation, the development, and the transport of stratospheric sulfuric acid aerosol. The aerosol size distribution and the sulfuric acid mass fraction are calculated as a function of the H_2SO_4/H_2O concentration, temperature, and air pressure in a size range between 0.001 μm and 2.58 μm. Binary homogeneous nucleation of H_2SO_4/H_2O, condensation and evaporation of H_2SO_4 and H_2O, Brownian coagulation and gravitational sedimentation are included. The microphysical model for stratospheric sulfate aerosol and a stratospheric sulfur chemistry are combined with a representation of the tropospheric sulfur chemistry. This tropospheric scheme accounts for the natural and anthropogenic emissions, chemistry, and dry and wet deposition of DMS, SO_2, and SO_4^{2-}. Globally and seasonally different SO_2- and SO_4^{2-} sources for stratospheric aerosol can therefore be taken into account. Results of a multiannual simulation show that the simulated SO_2 and H_2SO_4 concentrations are generally in good agreement with available observations. The formation of new particles through homogeneous nucleation takes place in the tropical lower stratosphere and upper troposphere and in polar spring. The aerosol surface area density and the aerosol mass concentration reproduce lower stratospheric background conditions quite well. Effective radius and aerosol mixing ratio agree also with satellite and in situ measurements at Northern Hemisphere midlatitudes.

1. Introduction

Stratospheric aerosol has various effects on the global climate system. It changes the chemical composition of the stratosphere because of heterogeneous reactions [*Hofmann and Solomon*, 1989], provides condensation nuclei for the formation of polar stratospheric clouds and cirrus, and disturbs the radiative balance of the atmosphere in changing the albedo [*Lacis et al.*, 1992]. These different atmospheric mechanisms are especially strong when the aerosol background layer is perturbed in response to strong volcanic eruptions or possibly in the future to high–speed civil transport aircraft. After the eruption of Mount Pinatubo (15.1°N, 120.4°E) in June 1991 a temperature increase in the lower stratosphere of ~ 2-3 K [*Labitzke and McCormick*, 1992] and a cooling of the global lower troposphere and the Earth's surface of ~ 0.5 K were detected [*Dutton and Christy*, 1992]. Furthermore, in 1992 and 1993 unusually strong ozone depletion due to chemical and dynamical processes was observed [*Grant et al.*, 1994; *Her-*

man and Larko, 1994; *Randel et al.*, 1995]. Stratospheric aerosol consists mainly of supercooled hydrated H_2SO_4 particles with a sulfuric acid mass fraction in the range of 50-80%. The particles form a persistent aerosol layer (Junge layer), which extends from the tropopause up to 30 km altitude. Height and maximum of the layer are seasonally and latitudinally dependent [*Yue and Deepak*, 1984]. The stratospheric aerosol particles are either directly formed in the stratosphere because of homogeneous nucleation or transported through the tropopause. In order to better understand the role of stratospheric aerosol in the atmospheric system several aerosol models were developed. At the end of the seventies, [*Turco et al.*, [1979] and [*Turco et al.*, [1979] developed a one-dimensional (1-D) model, which was later refined by *Toon et al.* [1988] and *Zhao et al.* [1995]. Recently, *Kärcher* [1998] developed a coupled microphysical–chemical–dynamical box trajectory model for aircraft-generated liquid aerosols, which could also be applied to liquid $H_2SO_4/HNO_3/H_2O$ aerosols. In the last years several studies with two–dimensional (2-D) chemistry transport models including sulfate aerosol microphysics were published in the literature. Theses studies focus on the impact of either aircraft emissions [*Bekki and Pyle*, 1992, 1993; *Pitari et al.*, 1993;

Weisenstein et al., 1996, 1998] or volcanic eruptions [*Tie et al.*, 1994; *Bekki and Pyle*, 1994; *Weisenstein et al.*, 1997] on the stratospheric aerosol distribution. These models could represent stratospheric back ground aerosol quite successfully. However, a model comparison between four different 2-D chemical transport models [*Weisenstein et al.*, 1998], which include sulfate aerosol microphysics, reveals differences in the simulated stratospheric aerosol background concentration. These differences seem to be mainly caused by transport processes [*Weisenstein et al.*, 1998]. Global transport directly affects the stratospheric aerosol distribution. Measurements and theoretical considerations with a 1-D model [*Brock et al.*, 1995, *Hamill et al.*, 1997] suggest that new particles are formed in the upper troposphere and then reach the stratosphere with ascending air. Prominent processes that lift lower tropospheric aerosols and aerosol precursor gases to the tropopause region are deep convective clouds in the tropics and warm conveyor belts (WCBs) in extratropical frontal systems. Both processes are small-scale events which are either not (WCBs) or only crudely (zonal mean) (deep convective clouds) resolved in 2-D models. Recently, *Pitari and Mancini* [2001] and *Pitari et al.* [2001] found with a three-dimensional (3-D) chemical-transport model study and an explicit treatment of aerosol dynamics that 43% of the stratospheric sulfate originates from carbonyl sulfide (COS) photolysis, 30% from upward transported sulfate and 27% from the oxidation of SO_2, which is transported into the stratosphere through the tropical tropopause. Transport seems to play an important role in the stratospheric aerosol budget. Thus, in order to better understand the formation and the development of stratospheric aerosol, 3-D model simulations with a much more realistic description of convective and advective transport processes are necessary. Here we will present the stratospheric aerosol model (SAM), which has been developed for application in the Hamburg climate model ECHAM4. ECHAM4 is a spectral general circulation model (GCM), with a radiation scheme which takes into account the effects of some aerosol components. This offers the possibility of investigating the various interactions between radiation, circulation, and chemistry and aerosol microphysics. Hence the role of stratospheric aerosol in the global climate system can be studied. Furthermore, the global calculation of aerosol dynamics provides a necessary model basis to interpret and interpolate observational aerosol data that are irregularly distributed in time and space. This is especially important in the view of upcoming satellites, e.g., ESSP3-CENA. In this paper, we will introduce the first version of the 3-D stratospheric aerosol model SAM and present results of a multiannual background simulation. The main focus of this paper lies in the comparison of simulated aerosol properties with different observations from the stratospheric background periods 1978/1979

and 1989 - 1991. We will discuss the model results and outline further improvements.

2. Model Description

The global stratospheric aerosol model SAM consists of two parts, a microphysical stratospheric aerosol model [*Timmreck and Graf*, 2000] and an atmospheric sulfur chemistry scheme, which are both implemented in the Hamburg climate model ECHAM4 [*Roeckner et al.*, 1996]. Using a sigma-hybrid coordinate system, the ECHAM4 model is divided into 19 layers from the Earth's surface to the pressure level of 10 hPa. The ECHAM4 model itself is based on primitive equations with vorticity, divergence, (logarithm of) surface pressure, temperature, water vapor, and cloud (liquid and ice) water content as prognostic variables. In our model simulations, ECHAM4 is integrated with a spectral triangular truncation at wave number 30 (T30 resolution). Physical processes and nonlinear terms are calculated on a Gaussian longitude–latitude grid with a nominal resolution of 3.75° × 3.75°. In the model a semi Lagrangian transport scheme [*Williamson and Rasch*, 1989] is applied for the tracer transport. A semi–implicit leapfrog time integration is used with a time step of 30 min for both the dynamics and the physics, while the radiation and diabatic heating rates are calculated every 2 hours. Previous studies with the ECHAM model [*Steil et al.*, 1998] showed that the coupled model satisfactorily describes important features of the lower stratosphere chemistry and dynamics, although the meridional poleward transport in the lower stratosphere is overestimated [*Timmreck et al.*, 1999].

2.1. Sulfur Chemistry Scheme

For ECHAM a tropospheric sulfur scheme has been developed by *Feichter et al.* [1996] which simulates the oxidation pathways of sulfur dioxide (SO_2) and the removal processes of SO_2 and sulfate (SO_4^{2-}) in the troposphere. This sulfur scheme includes transport, emission, chemistry, and wet and dry deposition of dimethyl sulfide (DMS), SO_2, and SO_4^{2-}. The sulfate aerosol is described with a bulk approach with no additional information about its size distribution. In the gas phase, SO_2 and DMS react with OH whereby the only end product of DMS oxidation is assumed to be SO_2. SO_2 is then dissolved in cloud water and oxidized by both hydrogen peroxide (H_2O_2) and ozone (O_3). The dissolution and the dissociation coefficients of SO_2 in cloud water are calculated according to Henry's law. The dry deposition of SO_2 and SO_4^{2-} is parameterized according to *Ganzeveld et al.* [1998] as a function of the concentration in the lowest model layer and of a prescribed dry deposition velocity. For SO_2 the deposition velocity is assumed to be 0.2 cm s^{-1} over land, 0.1 cm s^{-1} over snow and sea ice, and 0.8 cm s^{-1} over water and wetted surfaces. For sulfate aerosols the values are

Table 1. Sulfur Emission

	Species	Source	Reference	Mt S/a
Natural	DMS	marine biosphere	*Bates et al.* [1987]	18.1
	DMS	terrestrial biosphere	*Spiro et al.* [1992]	0.9
	SO_2	silent degassing and eruptive volcanoes	*Spiro et al.* [1992] *Graf et al.* [1997]	8.0
Anthropogenic	SO_2	biomass burning	*Hao et al.* [1990]	2.5
	SO_2	fossil fuel use and industry	*Benkovitz et al.* [1994]	66.8
Sum				96.3

0.025 cm s^{-1} for land, snow, and sea ice and 0.2 cm s^{-1} for wetted surfaces (H. Feichter, personal communication, 1998). The uptake of soluble sulfur species in cloud droplets (in-cloud scavenging), is calculated in terms of the model's precipitation formation rate [*Giorgi and Chameides,* 1986]. The wet removal of SO_2 and SO_4^{2-} below clouds (below-cloud scavenging) is parameterized according to *Berge* [1993]. Anthropogenic and volcanic emissions are released as SO_2, and biogenic emissions are released as DMS. Table 1 provides an overview of the emission scenario. For a detailed description of the model, see *Feichter et al.* [1996]. In their work, *Feichter et al.* [1996] showed that the annual mean surface concentration of SO_2 and SO_4^{2-} as well as the SO_4^{2-} concentration in precipitation agree with the observed annual values within a factor of 2. The global distribution of sulfate in the troposphere reflects the source strength of the anthropogenic emissions with maxima over east Asia, central Europe, and the North American east coast. In the Southern Hemisphere the influence of biomass burning can be detected, but the sulfate distribution of the Southern Hemisphere is dominated primarily by biogenic sources. In order to describe the formation and evolution of stratospheric aerosols a stratospheric sulfur chemistry scheme is required on the top of the tropospheric scheme. *Timmreck and Graf* [2000] parameterized the stratospheric sulfur chemistry in a very simple way. Now a more sophisticated approach is applied for the global simulation. The reactions that are considered are summarized in

Table 2. Monthly mean oxidant concentrations are prescribed from ECHAM calculations with a comprehensive chemical model [*Roelofs and Lelieveld,* 1995] except OH which is taken from a 12 year ECHAM3 feedback run with homogeneous and heterogeneous chemistry [*Steil et al.,* 1998]. For the COS concentration and the photolysis rate we use monthly mean fields from a 2-D simulation [*Grooß et al.,* 1998].

2.2. Microphysical Stratospheric Aerosol Model

A stratospheric aerosol model has been included in the ECHAM model [*Timmreck,* 1997]. This model treats the formation and the development of stratospheric sulfuric acid aerosol as a function of the sulfuric acid vapor and water vapor concentration, temperature, and pressure. The aerosol size distribution is separated into discrete size bins with a bin width which is determined by mass doubling [*Kritz,* 1975]. The original version used by *Timmreck and Graf* [2000] treats 44 aerosol size bins ranging from $3 \times 10^{-4} \mu$m to 6.2 μm. In ECHAM a less expensive version is implemented with 35 bins covering the $1 \times 10^{-3} \mu$m to 2.58 μm range. *Timmreck* [1997] showed that the differences between the two model simulations are relatively small. The microphysical processes, which are included in the model, are the following: binary homogeneous nucleation of H_2SO_4/H_2O, condensation and evaporation of H_2SO_4 and H_2O, Brownian coagulation, and gravitational sedimentation. The formation of new particles

Table 2. Stratospheric Sulfur Chemistry

Photolytic Reaction	λ [nm]
$SO_2 \xrightarrow{h\nu} SO + O$	$\lambda < 220$
$COS \xrightarrow{h\nu} CO + S$	$\lambda < 260$
Gas Phase Reaction	**Reaction rate [cm^{-3} s^{-1}]**
$S + O_2 \longrightarrow SO + O$	$R_{S1} = 2.3 \, 10^{-12}$
$SO + O_2 \longrightarrow SO_2 + O$	$R_{S2} = 2.6 \, 10^{-13} \exp(-2400/T)$
$COS + O \longrightarrow SO + CO$	$R_{S3} = 2.1 \, 10^{-11} \exp(-2200/T$
$COS + OH \longrightarrow$ products	$R_{S4} = 1.1 \, 10^{-13} \exp(-1200/T)$
$SO_2 + OH \xrightarrow{M} HSO_3$	$R_{S5} = f(K_0, K_\infty)$ $K_0 = 3.0 \, 10^{-31} (T/300)^{-3.3}$ $K_\infty = 1.5 \, 10^{-12}$
$HSO_3 + O_2 \longrightarrow SO_3 + HO_2$	$R_{S6} = 1.3 \, 10^{-12} \exp(-330/T)$
$SO_3 + H_2O \longrightarrow H_2SO_4$	$R_{S7} = 6.0 \, 10^{-15}$

due to binary homogeneous nucleation of H_2SO_4 and H_2O is calculated according to classical theory. The size of the freshly nucleated particles is smaller than the smallest size bin, and this mass is put into the first size bin. The lower end of the size distribution is therefore shifted to fewer but larger particles. Condensation and evaporation of H_2SO_4 and H_2O on the aerosol particles is calculated differently. It is assumed that the water vapor pressure over the H_2O/H_2SO_4 droplet is always in equilibrium with the H_2O partial pressure and that condensation/evaporation of the water molecules occurs instantaneously. Condensation (evaporation) of H_2SO_4 on the aerosol particles is considered as advection in the radius space, and the growth rate is interpreted as radial velocity. For the numerical solution of the sulfuric acid condensation the advection scheme of *Chlond* [1994] is used. An important parameter for the H_2SO_4 condensation on the aerosol particles, especially for small particles, is the sticking coefficient α. Here α is defined as the ratio of the number of H_2SO_4 molecules which are incorporated in the aerosol after a collision and the total number of gaseous H_2SO_4 molecules, which collided with the aerosol particle. Laboratory experiments under normal conditions [*Van Dingenen and Raes*, 1991] have quantified a sticking coefficient in the range $0.028 < \alpha < 0.064$ with an average value of $\alpha = 0.04$, while theoretical considerations [*Clement et al.*, 1996] led to a value of unity. Our box simulations have shown significant differences in the model results dependent on the choice of α. Therefore we have performed two different model runs, one with a sticking coefficient of $\alpha = 1$ and a second with $\alpha = 0.04$, in order to investigate the influence of α on the aerosol distribution. We will discuss these results in section 3. Changes in the particle size distribution due to Brownian coagulation are calculated with the coagulation kernel according to *Fuchs* [1964]. The particle loss in every size bin i due to gravitational sedimentation is modeled by a sink term proportional to sedimentation velocity and aerosol number density and inversely proportional to the height of the model layer. A detailed model description is given by *Timmreck and Graf* [2000]. They show that box simulations of the microphysical model were able to reproduce the formation and the development of stratospheric aerosol in the undisturbed and disturbed atmosphere. The calculated aerosol size distributions agree quite well with the observations, and the temporal development after a volcanic eruption could also be reproduced by the model.

In the first version of the global stratospheric aerosol model SAM, which is introduced here, the microphysical model is only applied to the upper nine layers of the global model (10-300 hPa). Three-dimensional simulations of stratospheric aerosol require a large amount of computing time. In order to test the model and to obtain results in a reasonable time period, the microphysical model is only integrated in the stratospheric and upper tropospheric layers of the model. The aerosol size-resolving component in the stratosphere and the aerosol bulk approach in the troposphere are coupled by the total aerosol mass mixing ratio (SO_4^{2-}). SO_4^{2-} is the only aerosol variable which is available throughout the model domain. While the microphysical processes are integrated separately in time for each size bin, all bins are considered together for the advection process: The total aerosol mass is transported as a bulk. After every advection time step the aerosol mass of each size bin is scaled with the ratio of the total aerosol mass after and before advection. For the advective transport I therefore assume that the gradients of the different size bins do not differ much and that the aerosol size distribution in adjacent grid boxes is similar to a first approximation. This assumption is only applied in the upper model layers, where the aerosol transport is determined by large-scale advection and where small-scale processes like convection are not relevant. The big advantage of this method is the saving of a large amount of computing time (3% for each additional tracer). The simplification will, however, lead to some numerical diffusion in particular in the vertical, where the tracer gradients of small and large particles are different because of gravitational sedimentation. We conduct two model runs with SAM one with $\alpha=1$ and one with $\alpha=0.04$, both over an 8year period, but consider only the last 5 years for the analysis.

3. Results

3.1. Precursor Gases

COS, SO_2, and H_2SO_4 (g) are the atmospheric precursor gases of the stratospheric sulfuric acid aerosol. While the monthly mean values of the COS concentration are prescribed, the SO_2 and H_2SO_4 (g) concentration are explicitly calculated. Figure 1 shows a comparison of a 5 year average of the SO_2 volume mixing ratio calculated with the full sulfur chemistry scheme of this study and an ECHAM simulation with tropospheric sulfur chemistry only. In contrast to the tropospheric sulfur chemistry simulation the global aerosol model has a local minimum in the lowermost stratosphere, which is most pronounced in the tropics. The increase with height in the SO_2 mixing ratio above 18 km results from the consideration from COS photolysis. Similar SO_2 profiles are obtained by other model simulations [*Weisenstein et al.*, 1997; *Zhao et al.*, 1995]. *Weisenstein et al.* [1997] obtained a tropical minimum in the SO_2 mixing ratio of $\sim$ 5.5 pptv at 18 km which is consistent with our model results. For the Northern Hemisphere midlatitudes, *Weisenstein et al.* [1997] estimate a lower SO_2 mixing ratio (2 parts per trillion by volume (pptv)) than at the equator, whereas in our simulation the midlatitude SO_2 mixing ratio (7.5 pptv) is higher than in the tropics. One reason for this difference might be the different parameterizations which are
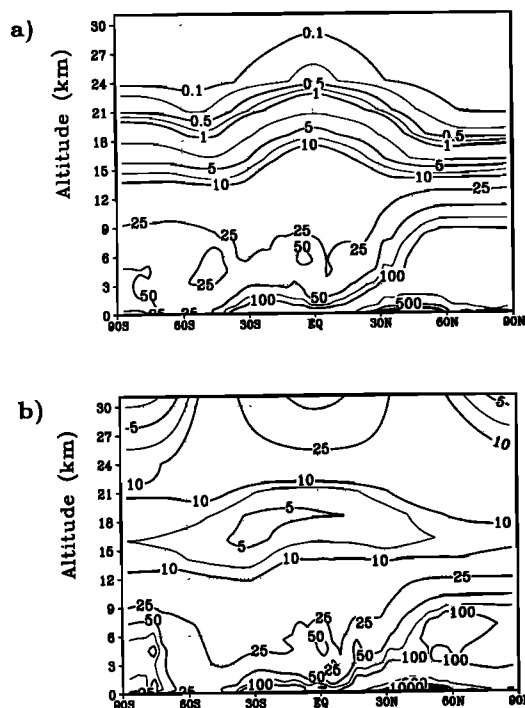
Figure 1. Latitude-altitude cross section of the zonally averaged SO$_2$ concentration (pptv)(5 year mean) for (a) tropospheric sulfur chemistry only and (b) the global aerosol model including stratospheric sulfur chemistry.

used for the tropospheric removal rate of SO$_2$. Weisenstein et al. impose a fixed tropospheric wet removal rate of SO$_2$, while in our model the loss processes (heterogeneous reaction with H$_2$O$_2$ and O$_3$ in cloud and below

cloud scavenging) are explicitly calculated. Another possible reason might be differences in the transport modeling. Model intercomparisons [e.g. *Danilin et al.*, 1998] have found large differences in the stratospheric-tropospheric exchange between 2-D and 3-D models and even between 3-D models.

Unfortunately, only a few SO$_2$ measurements from the upper troposphere and lower stratosphere are available to validate the model results. Vertical SO$_2$ profiles between 67°N and 60°S and between 1and 12 km altitude were derived by *Ockelmann and Georgii* [1989] from aircraft measurements made in June 1984. They found SO$_2$ mixing ratios between 20 and several 100 pptv with local maxima in the upper troposphere above 200 pptv in the Southern Hemisphere and 300 pptv in the Northen Hemisphere. The model is able to reproduce a local maximum in the middle and upper troposphere in the Northern Hemisphere midlatitudes although the zonally maximum value is lower than observed. Simulated daily values (not shown), however, could be about factor of 2 larger. In Figure 2 the simulated SO$_2$ mixing ratios are compared with measurements from the Max Planck Institute Heidelberg, at Kiruna (68°N) in February 1987 [*Möhler and Arnold*, 1992] and in the vicinity of Teneriffe (28°N) in July 1997 [*Curtius et al.*, 1998]. In general, it is difficult to compare in situ measurements taken at one point under specific synoptic conditions with climate model simulations with a nominal resolution of 320 km × 320 km. In Figure 2 the error bars indicate the simulated maximum and minimum SO$_2$ values at the corresponding grid boxes and altitudes in the simulated time frame (5
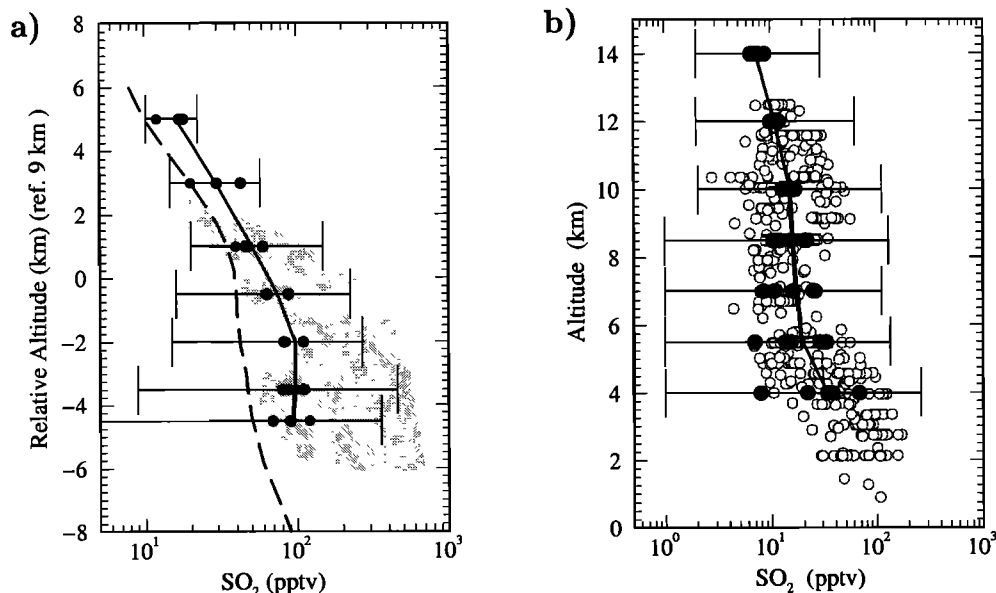

Figure 2. Comparison of simulated SO$_2$ data (pptv) with in situ measurements (a) at Kiruna and (b) near Teneriffe. In Figure 2a the shaded area indicates the measurements by *Möhler and Arnold* [1992], and the solid circles indicate the model results. In Figure 2b the open circles indicate measurements by *Curtius et al.* [1998] during the ACE II campaign, and the solid circles indicate the model results. The error bar indicate the range of variability.

years). This large variability, in particular for the troposphere, makes a comparison between model results and observations quite difficult. Hence we will compare the observations to monthly averaged values, which also, but to a lesser extent than the daily values, reflect the atmospheric variability (interannual). At Kiruna (68°N) the simulated monthly averaged SO_2 mixing ratios are in quite good agreement with the observations in the troposphere and around the tropopause, whereas in the stratosphere model results and observations differ significantly. The simulated vertical profile decreases only slightly above the tropopause (-10 pptv km^{-1} within 2 km), while the measurements show a much stronger gradient (-50 pptv km^{-1}). A possible reason for this could be strong numerical diffusion in the model which is enhanced in the applied semi-Lagrangian transport scheme when large tracer gradients appear [*Timmreck et al.*, 1999]. A similar slight stratospheric decrease in the SO_2 mixing ratio as in our model is, however, simulated with a 1-D profile [*Turco et al.*, 1981], although this model underpredicts the tropospheric SO_2 values significantly. Other published SO_2 measurements at 68°N [*Inn et al.*, 1981] are much higher with values between 36 and 51 pptv at 15 km. SO_2 measurements [*Meixner*, 1984] which were taken between 10 and 12 km and at 40°-60°N range between 10 and 59 pptv with different vertical gradients above the tropopause in the range from -1.2 pptv km^{-1}

to +16.5 pptv km^{-1}. Between 8 and 12 km and 54°-67° N, *Ockelmann and Georgii* [1989] observed SO_2 mixing ratios in the range of 40-200 pptv with vertical gradients from 0 pptv km^{-1} to +10 pptv km^{-1}. Hence the observational basis for model evaluation is extremely weak especially for high latitudes, where day to day variability is strong due to the influence of synoptic activity.

In the vicinity of Teneriffe (28°N) the simulated monthly averaged SO_2 mixing ratio profiles also agree quite well with observations, which were taken during the ACE II field campaign. At all altitudes the model results are within the observational range. Above 10 km the model results for every year are quite similar, but below 10 km a strong interannual variability is simulated. In contrast to the vertical SO_2 profile at high latitudes both measurements and model results show only a slight decrease with altitude. In general, more measurements at different latitudes and seasons would be necessary to get a more complete picture of stratospheric SO_2 concentration. In contrast to the SO_2 concentration, which is not influenced by the choice of the sticking coefficient α, the atmospheric H_2SO_4 (g) concentration is strongly dependent on α. In box simulations with the microphysical model [*Timmreck and Graf*, 2000] the equilibrium H_2SO_4 concentration for an assumed sticking coefficient of $\alpha = 0.04$ was about a factor of 2-3 higher compared to the one determined with $\alpha = 1$. The contribution of the condensation process
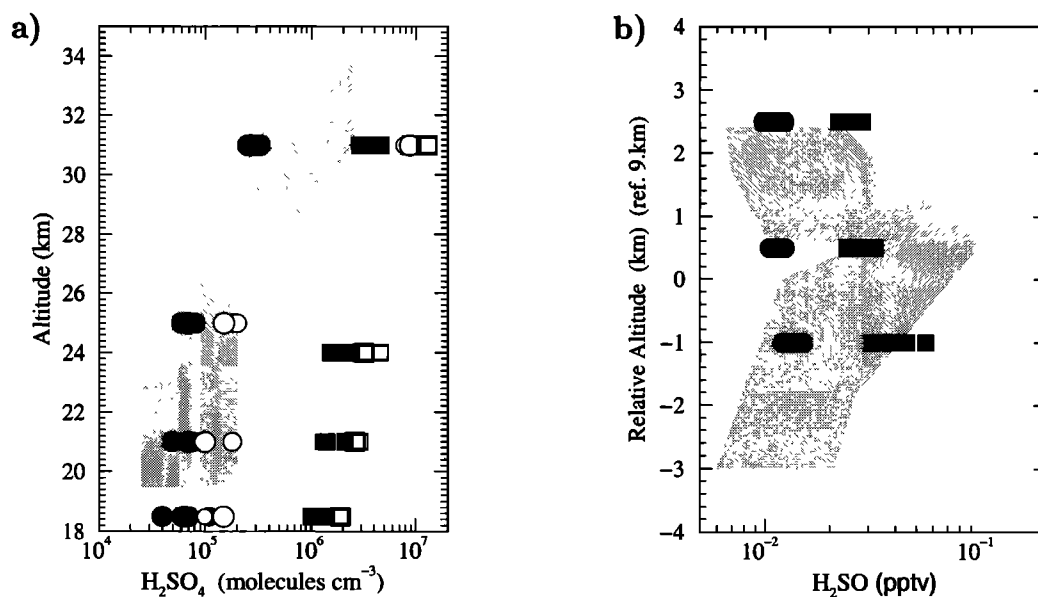

Figure 3. (a) Simulated sulfuric acid vapor concentration (molecules cm^{-3}) at Northern Hemisphere midlatitudes (44°N) for two different months June (open symbols) and October (solid symbols). Circles denote model results for $\alpha = 1$, and squares denote results for $\alpha = 0.04$. The shaded area indicates the range of observations in June 1982, and the hatched area indicates the range of observations in September/October 1981 according to *Arnold and Bührke*, [1983]. (b) Comparison of the simulated H_2SO_4 volume mixing ratio (parts per trillion by volume) with in situ measurements at Kiruna. The shaded area indicates the measurements by *Möhler and Arnold* [1992], the solid circles indicate the simulations for $\alpha = 1$ and the solid squares indicate the simulations for $\alpha = 0.04$.
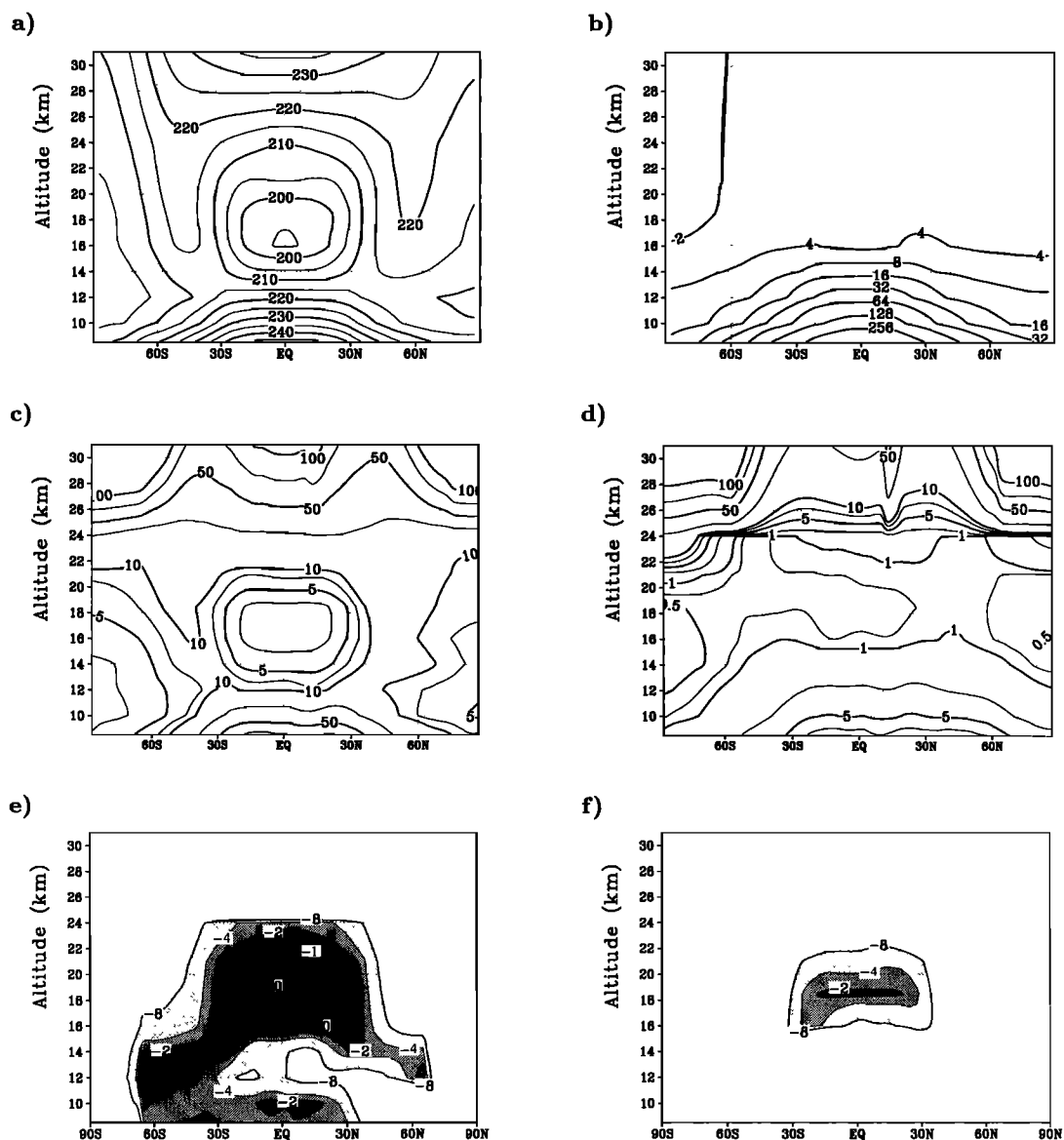
Figure 4. Latitude-altitude cross section (5 year average) of calculated (a) temperature (K), (b) specific humidity (ppbm), (c) $H_2SO_4(g)$ $(10^5$ $cm^{-3})$ for $\alpha = 0.04$, (d) same for $\alpha = 1$, (e) logarithm of the nucleation rate $(cm^{-3}$ $s^{-1})$ for $\alpha = 0.04$, and (f) same for $\alpha = 1$.

to the aerosol formation is different for both assumptions. In the simulation with $\alpha = 1$ many more (25 times) H_2SO_4 molecules are incorporated in the aerosol particles. However, the simulated sulfuric acid vapor concentrations in the box model were overestimated for all cases compared to the observations, which was mainly explained with the neglect of tropospheric particles [*Timmreck and Graf*, 2000]. In Figure 3a the simulated H_2SO_4 (g) concentrations at Northern Hemisphere midlatitudes for a sticking coefficient of $\alpha = 1$ and of $\alpha = 0.04$ are compared to observations [*Arnold and Bührke*, 1983]. The observed data include balloon measurements from September and October 1981 and from June 1982, while the simulated data are given by the corresponding monthly mean values for each year.

Both simulations and observations show a similar behavior with smaller values in October than in June. The model simulation can reproduce the observed seasonal and vertical variability quite well. Differences between both model runs occur in the estimated quantities and in the H_2SO_4 gradient at the top of the aerosol layer. The simulated H_2SO_4 (g) concentration for an assumed sticking coefficient of $\alpha = 1$ (circles) are in the observed range, whereas the simulations with $\alpha = 0.04$ (squares) clearly overestimate the observed concentration by a factor of 10. Furthermore, the strong increase in the observed H_2SO_4 (g) concentration above 25 km is reproduced much better with a sticking coefficient of unity. At Kiruna (68°N) the simulated H_2SO_4 mixing ratios for both model runs are in the observed range

2.5 km above and 1 km below the tropopause as the comparison of simulated data with measurements from February 1987 [*Möhler and Arnold*, 1992] shows (Figure 3b). While the values for $\alpha = 1$ are clearly within the observational range, the values for $\alpha = 0.04$ are at the upper end of the observation. Just above the tropopause the model is not capable of reproducing the sharp observational peak, possibly because of strong numerical diffusion. At this altitude the values for $\alpha = 1$ are about a factor of 4 smaller than the observations, while the values for $\alpha = 0.04$ are at the lower edge of the observational range. Overall, the simulated SO_2 and H_2SO_4 (g) concentrations agree quite well with the observations. However, at present, only a few atmospheric measurements of sulfur-containing gases exist. More measurements at different sites are desirable to better validate the model results.

3.2. Homogeneous Nucleation

New particles can be formed in the atmosphere through binary homogeneous nucleation of H_2SO_4/H_2O. Figure 4 shows the global distribution of the nucleation rates of the sulfuric acid vapor concentration for both model runs and of the temperature and water vapor concentration. Owing to the lower H_2SO_4 (g) concentration in the model run with $\alpha = 1$, fewer H_2SO_4 molecules are available for the nucleation of new particles. This leads to lower nucleation rates with maximum values of $\sim 10^{-2}$ s^{-1} cm^{-3} compared to 1 s^{-1} cm^{-3} for the simulation with $\alpha = 0.04$ (Figure 4).

Although the amount of the H_2SO_4 (g) concentration influences the strength of the nucleation, the occurrence of the homogeneous nucleation is mainly determined by the temperature. Hence, in both model runs, the formation of new particles through homogeneous nucleation takes place preferably in the tropics around 17 km, where the coldest temperatures in the model occur. Measurements and 1-D model simulations by *Brock et al.* [1995] suggest that homogeneous nucleation in the upper tropical troposphere is the main source for new stratospheric aerosol particles. In contrast to the findings by *Brock et al.* [1995] the simulated maximum of the tropical nucleation rate is located in the lower tropical stratosphere and not in the upper tropical troposphere. In ECHAM4 the temperature values in the upper tropical troposphere are ~ 2 K too high compared to European Centre for Medium-Range Weather Forecasts–analysis data and in the tropical stratosphere are ~ 2-4 K too low [*Roeckner et al.*, 1996]. This model bias, which is a common feature of general circulation models, might explain the differences to the measurements by *Brock et al.* [1995] and emphasizes the important role of the temperature in the nucleation process.

Measurements [*Wilson et al.*, 1989] and simulations [*Zhao*, 1993] suggest that enhanced homogeneous nucleation also takes place in polar spring. In Figure 5 the logarithm of the nucleation rate for April and October is
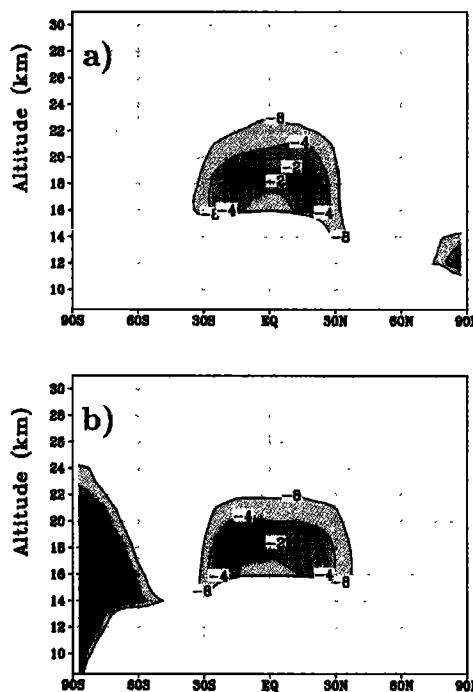

Figure 5. Global distribution of the homogenous nucleation rate ($\log_{10}$ J (cm^{-3} s^{-1})) in the model run with a sticking coefficient of $\alpha = 1$ in (a) April and (b) October.

shown for the model run with a sticking coefficient of 1. In both months a second local maximum occurs at the winter pole in good agreement with the observations. Owing to the colder temperatures the maximum at the South Pole is much more pronounced than the one at the North Pole. A similar picture can be found for the simulation with $\alpha = 0.04$, but the nucleation rates are higher than for $\alpha = 1$. Overall, the 3-D aerosol model is able to reproduce most of the features observed in particle production. The nucleation rates differ by ~ 2 orders of magnitude between both model runs, which is quite small compared to the theoretical and experimental uncertainties. However, the model run with $\alpha = 1$ seems to be more realistic because of the better agreement of the sulfuric acid vapor concentration with the observations (Figure 3).

3.3. H_2SO_4 Number Density

In Figure 6 the simulated vertical distribution of the total (gas plus aerosol) sulfuric acid concentration at Northern Hemisphere midlatitudes in October is compared with observations for the corresponding month [*Arnold et al.*, 1998]. In contrast to the comparison for the gaseous H_2SO_4 concentration alone (Figure 3), no significant differences between both model runs can be detected in the total H_2SO_4 concentration. The percentage of the gaseous fraction of the total sulfuric acid number density is $< 5\%$ for $\alpha = 0.04$ and is even smaller for $\alpha = 1$. For the simulation of the aerosol H_2SO_4 number density or the sulfuric acid aerosol mass, the
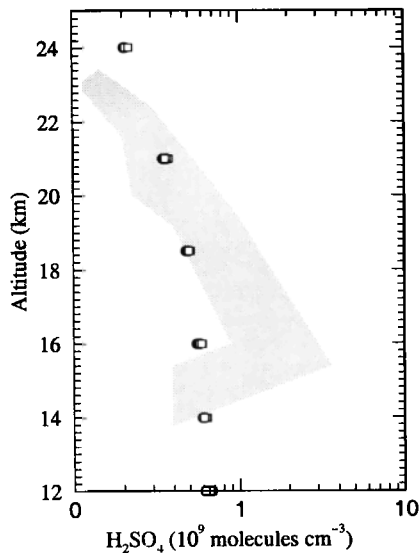
Figure 6. Vertical profile of the total (gas and aerosol) sulfuric acid concentration (10^9 molecules cm^{-3}) at Northern Hemisphere midlatitudes (44°N) in October. The solid circles denote simulations for $\alpha = 1$, and the open squares denote the simulations for $\alpha = 0.04$. The shaded area indicates the range of observations according to *Arnold et al.* [1998].

value of the sticking probability α is of less importance. This is in contrast to our previous box model results [*Timmreck and Graf*, 2000], where the nucleation process was the only source for particle formation in the atmosphere. Hence, without further notice, only model results with a sticking coefficient $\alpha = 1$ are shown in the following, because the aerosol properties do not differ significantly between both model runs.

The simulated values, in general, agree reasonably well with the observations. At 24 km the simulated

H_2SO_4 number density is about a factor of 2 higher and at 16 km is a factor of 2 lower than the observation. The observations show, however, a much stronger gradient than the model results. A possible reason for this discrepancy could be the numerical diffusion in the model. The numerical diffusion is as aforementioned, in general, enhanced in the applied semi–Lagrangian transport scheme when tracer gradients become large. Another reason might be the representation of stratospheric transport in the model. This will be discussed in section 3.4.

3.4. Aerosol Mass Mixing Ratio

In Figure 7 the temporal development of the aerosol mixing ratio over the simulated 5 years is shown at 30, 24, and 21 km. A noticeable difference between the three layers is the existence of the tropical aerosol reservoir in the two upper model layers (30 and 24 km). Analysis of SAGE data by *Trepte and Hitchman* [1992] show that the tropical stratosphere below 20 km is characterized by fast meridional poleward transport, while between 20°S and 20°N and between 20 and 28 km a tropical stratospheric reservoir (TSR) exists. The TSR has a distinctly different air mass than the midlatitude stratosphere. Possible reasons for the TSR are subtropical, quasi–permeable barriers with strong potential vorticity gradients, which inhibit transport of tropical air into the subtropics [*Haynes and McIntyre*, 1987; *Trepte and Hitchman*, 1992]. Observations in particular after the Mount Pinatubo eruption [e.g., *Trepte et al.*, 1993; *Grant et al.*, 1996] show that the TSR is a temporary reservoir for tropical aerosols. The tropical aerosol reservoir is controlled by the phase of the quasi-biennial oscillation (QBO) [*Trepte and Hitchman*, 1992; *Hitchman et al.*, 1994]. During the QBO easterly shear the
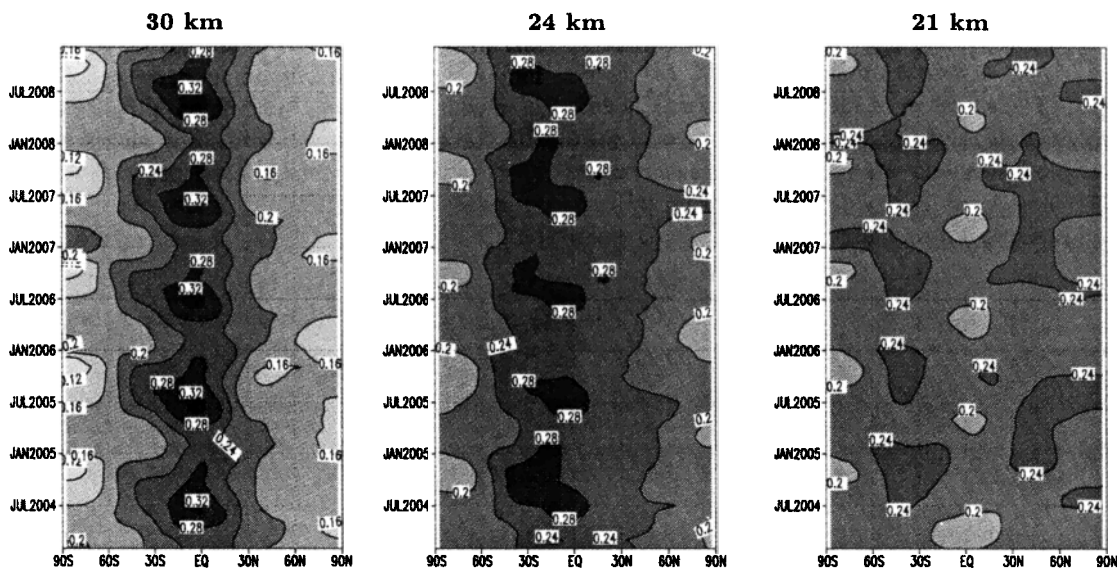

Figure 7. Temporal development of the calculated aerosol mixing ratio (ppb S) over the simulated 5 year period at 30, 24, and 21 km. The first 3 years of the model simulation are disregarded.
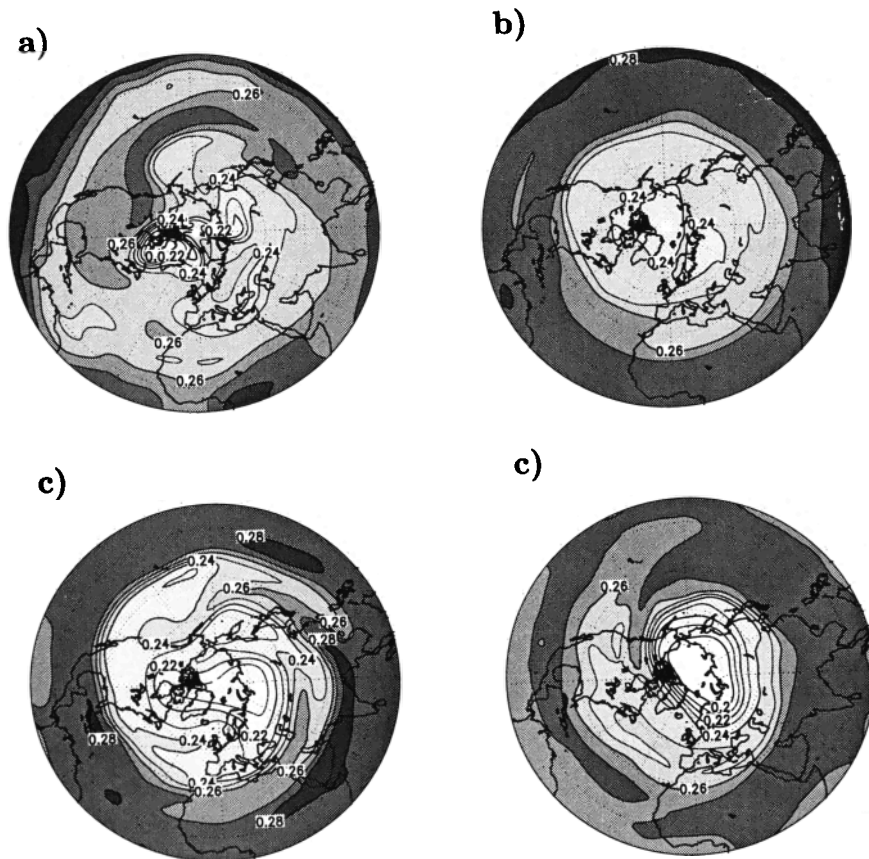
Figure 8. Northern Hemisphere polar stereographic distribution of the aerosol mixing ratio (ppb S) for (a) February 15, (b) May 15, (c) August 15, and (d) November 15, in model year 7.

tropical aerosol tends to remain near the equator, while during the westerly shear the aerosol tends to spread poleward. In the ECHAM model, as in all GCMs, the tropical winds are stable easterly. Thus the model is not capable of simulating the observed interannual variability of the tropical stratospheric aerosol which is associated with the QBO. Furthermore, it has to be taken into account that the model top layer is located at 10 hPa and acts as a sponge layer. Thus the aerosol concentration in the uppermost layer is not very representative of reality and should not be considered for a detailed analysis. The model results show however, a clear interannual and interseasonal variability at all heights. In the two upper model layers a local maximum occurs in early boreal summer in the tropics because of an increase in the COS concentration in spring. The lowest values are found at 30 km and at 24 km at high latitudes in polar spring. This springtime cleansing associated with the subsidence of the aerosol particles within the polar vortex has been observed in the Arctic [*Kent et al.*, 1985] and the Antarctic [*Thomason and Poole*, 1993].

Aerosol transport from the tropics to the high latitudes occurs in the middle stratosphere mainly as discrete events in planetary-scale tongues which are associated with an episodic amplification of planetary-scale waves in high latitudes of the winter hemisphere propa-

gating at the edge of the polar vortex [*Chen et al.*, 1994; *Waugh*, 1996]. Figure 8 shows the northern hemispheric distribution of the aerosol mass mixing ratio (ppb S) at 24 km on 4 days (fifteenth of each month) in model year 7. Synpotic-scale tongues originating in the tropics are clearly evident in the winter months but they are also visible in August (Figure 8c) when the vortex in the model starts to build up again. In February (Figure 8a) aerosol-rich air from the tropics is transported poleward and eastward around the displaced polar vortex, while aerosol-poor polar air is advected equatorward and westward. A similar pattern was found by *Harvey et al.* [1999] in Stratospheric Aerosol Measurement II observations. The analyzed data show that aerosol rich-air mass from Africa is transported eastward around the polar vortex into the Aleutian High. A minimum of aerosol-poor air characterizes a relatively zonal polar vortex in November (Figure 8d) which is surrounded by filaments with aerosol-rich air in the midlatitudes. The quiescent period is in May (Figure 8b), when the aerosol mass mixing ratio is organized in zonal bands.

The aerosol distribution at 21 km in Figure 7 looks quite different from the two upper layers. In the tropics, local minima exist in spring after the breakdown of the polar vortex. The aerosol mixing ratio at this altitude is therefore characterized by fast meridional transport of
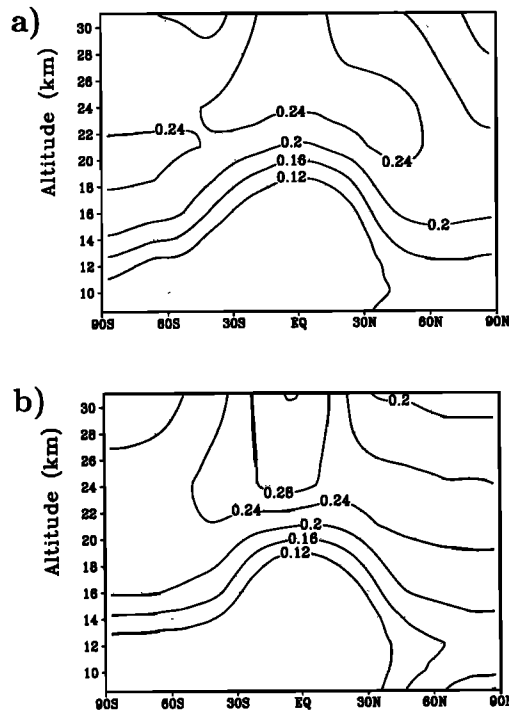
a)

b)

Figure 9. Latitude-altitude cross section of the calculated monthly averaged aerosol mixing ratio (ppb S) for (a) February and (b) May in model year 7.

Figure 10. Zonally averaged aerosol mass concentration (μg m^{-3}) between 35°N and 45°N at three different altitudes.

the lower transport regime. This is also apparent in the meridional cross sections for February (year 7) and for May (year 7) in Figure 9. In February (Figure 9a), the aerosol is confined in the tropics while after the breakdown of the polar vortex in May (Figure 9b) it is spread poleward. Our model shows that although both transport regimes exist in the model, most of the transport takes place in the lower transport regime as a result of the missing upper branch of the Brewer Dobson circulation. With the model version used a detailed analysis of the connection between spatial aerosol distribution and stratospheric circulation is therefore not feasible. As a consequence, we have to state that GCMs with a top at only 10 hPa are generally not useful to study such processes that involve transport of, e.g., stratospheric aerosols and/or ozone. In the following I will therefore
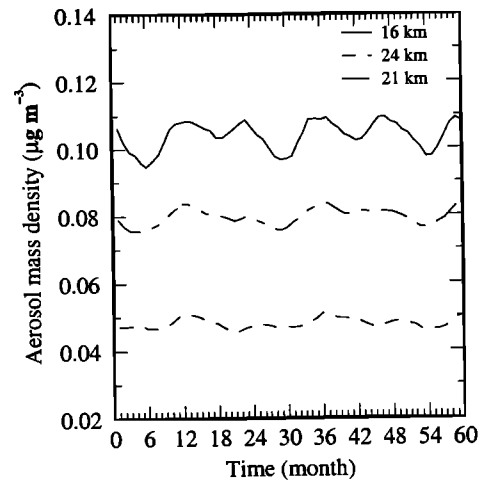
concentrate on the ability of SAM to simulate properties of the stratospheric aerosol size distribution, such as the aerosol number density and surface area density, in particular, for the Northern Hemisphere midlatitudes.

3.5. Aerosol Mass Density

In Figure 10 the zonally averaged aerosol mass density between 35°N and 45°N is shown for three different heights (16, 21, and 24 km). At 16 km a clear annual cycle is evident in the aerosol mass concentration, with a maximum in winter and a minimum in summer. This interannual variability is the result of stronger downward and poleward transport in the winter hemisphere. At 21 and 24 km the annual cycle is much less pronounced, although the model also shows a distinct interannual variability at these altitudes.

Our results agree quite well with the findings of *Thomason et al.* [1997a]. Analysis of Stratospheric Aerosol and Gas Experiment (SAGE) and SAGE II data by *Thomason et al.* [1997a] have shown that at northern midlatitudes a clear annual cycle is evident in the 1.02 μm aerosol extinction which is more pronounced at 15 km than at 20.5 and 25.5 km.

Table 3. Aerosol Mass Density

Time	Location	Stratospheric Data Intercomparison (μg m^{-3})	GCM Results (μg m^{-3})
1989	41°N; 18-to 22km altitude	0.10 OPC[a]; 0.19 SAGE II[b]	0.07-0.12
Dec. 1988	41°N; 19 km altitude	0.06 PCS[c]; 0.25 SAGE II[b]	0.11
Spring 1991	41°N; 17-to 21 km altitude	0.03-0.06 OPC[d]; 0.19 SAGE II[b]	0.08-0.12

[a] [*Hofmann*, 1990].
[b] [*Kent et al.*, 1995].
[c] [*Wilson et al.*, 1993].
[d] [*Deshler et al.*, 1993].

The simulated values of the aerosol mass density at Northern Hemisphere midlatitudes also agree quite well with observations. In Table 3, observed background values of the stratospheric data intercomparisons [*Kent et al.*, 1995] are compared with our global model results for the corresponding latitude and altitudes. With values between 0.07 and 0.12 μg m^{-3} the model results are within the range of the observations (i.e., 0.03-0.19 μg m^{-3}). The SAGE II data [*Kent et al.*, 1995] with values of $\sim$ 0.19-0.25 μg m^{-3} are about a factor of 2 higher than in situ measurements and model results. However, *Yue et al.* [1994] derived from SAGE II extinction data aerosol mass densities in the range of 0.08-0.10 μg m^{-3} for April 1991, which are closer to the other measurements by *Kent et al.* [1995] and to the model simulations.

3.6. Aerosol Size Distribution

Figure 11 shows the annually averaged aerosol number density as a function of the particle radius at three different altitudes (18.5, 21, 24 km) for the equator and Northern Hemisphere middle (44°N) and high latitudes (79°N). In the tropics a large number of small freshly nucleated particles can be found in the simulation, which is consistent with the pronounced occurrence of homogeneous nucleation in that region (Figure 4). A distinct peak of small particles is also present at high latitudes due to the formation of new freshly nucleated particles in polar spring. At 44°N the amount of small particles is minimal because at midlatitudes less nucleation occurs in the model. At all latitudes the number of small particles decreases with altitude, and the peak of the aerosol size distribution shifts to smaller radii as altitude increases.

Usually the stratospheric background aerosol is described with a monomodal distribution because there is little available information about the number density of small particles below 0.01 μm. However, distinct bimodal and trimodal size distributions were detected in the volcanically disturbed atmosphere where homogeneous nucleation is the dominant process. Under background conditions, *Wilson et al.* [1992] observed bimodal size distribution in the polar region above the tropopause. They also found bimodal size distributions in the tropical upper troposphere and lower stratosphere. These regions are also characterized by very low temperatures, which are preferred for homogeneous nucleation. Unfortunately, only few measurements of the stratospheric aerosol size distribution exist. Most of them correspond to volcanically disturbed years. A unique exception is the long-term stratospheric aerosol data set from the University of Wyoming. Since 1971, vertical profiles of stratospheric aerosol have been regularly collected at Laramie, Wyoming, (41°N, 105°5'W) [e.g., *Deshler et al.*, 1992, 1993; *Hofmann*, 1990].

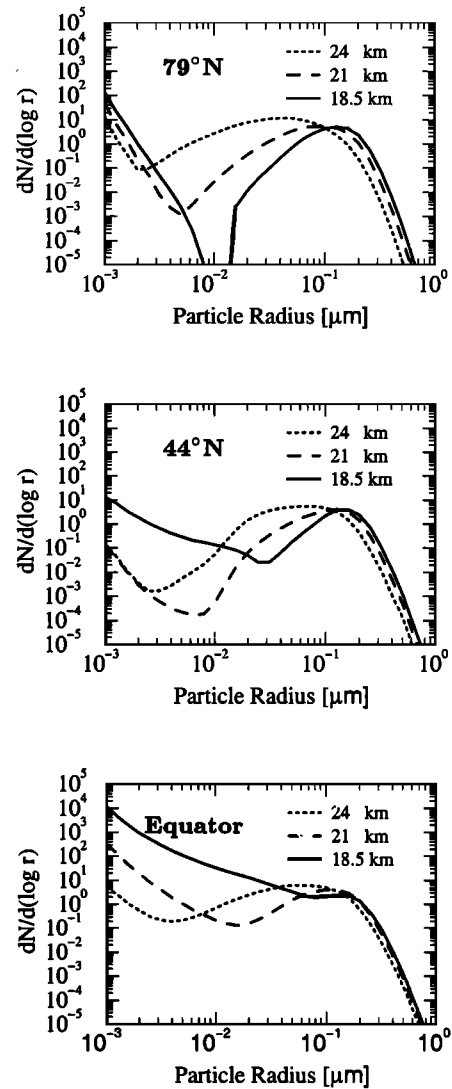The optical aerosol instruments which are used at Laramie measure the number concentration of aerosol

Figure 11. Aerosol number density $dN/d(logr)$ (N per cubic centimeters, r in microns) as a function of the particle radius at three different latitudes and altitudes.

in the size range 0.15 - 10 μm in eight size classes. In addition, a condensation nuclei (CN) counter is used to measure the number density concentration of particles with $r > 0.01$ μm. The measurements are fitted with a lognormal size distribution or a bimodal size distribution.

In Figure 12 we compare the simulated aerosol number density as a function of the particle radius at 24 km with balloon-borne aerosol measurements made at Laramie, Wyoming (T. Deshler, personal communication, 1999). For the measurements we have arbitrarily chosen four different days from the post-Pinatubo episode, one for each season. The simulated size distributions are monthly mean values for the grid box where Laramie is located. The simulations agree quite well with the measurements, especially for the larger particles with $r > 0.1$ μm. The model tends to underpredict very large particles in comparison to the obser-
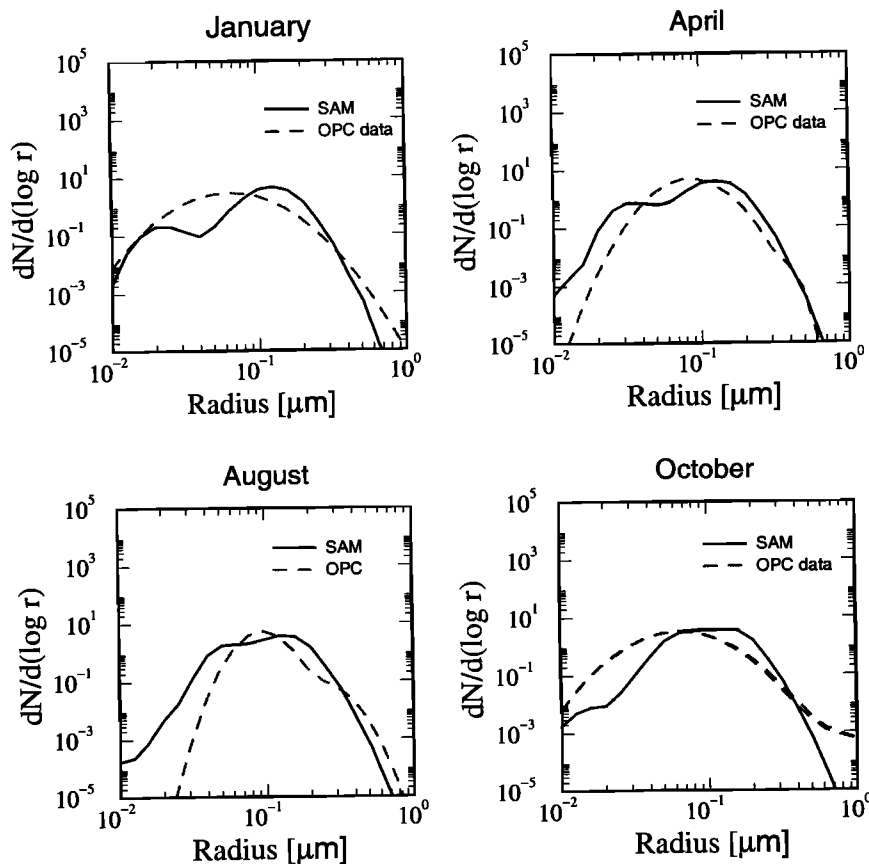
Figure 12. Size distribution of aerosol number density $dN/d(\log r)$ (N per cubic centimeters, r in microns) at 24 km and 41°N. The solid line shows monthly averaged model results of an arbitarily choosen model year, and the dashed line shows balloon-borne measurements at Laramie, Wyoming, on specific days from the post-Pinatubo episode.

vations, in particular, in October. The simulated and the observed aerosol number density differ for particles with $r > 0.7$ μm by > 2 orders of magnitudes. However, it could be possible that the observed particles contain some impurities such as ammonium sulfate and meteoric debris, so that they are larger than the pure sulfuric acid/water droplets. Model results and observations differ more substantially for the smaller particles $r < 0.1$ μm. In January the aerosol number density for particles with $r < 0.03$ μm agrees quite well with the optical particle counter (OPC) data, but the simulated values in April and August are $\sim$ 1-2 orders of magnitude higher than observed. The differences are especially pronounced in August where no particles with $r < 0.02$ μm are detected. The seasonal variability of number concentration with lowest values in August and highest in January is, however, well captured by the model.

The simulated size distributions show a bimodal structure with one peak between 0.01 μm and 0.05 μm and one around 0.15 μm. Whether this is realistic is difficult to assess. It has to be taken into account that the fitted observed size distribution in this specific size range is derived only from the numbers provided by the CN

counter. Owing to the low spectral resolution the observations cannot provide sufficient information to assess if the simulated size distribution is true or not. Measurements with a finer resolution below 0.1 μm are therefore desirable to validate the model simulations.

3.7. Aerosol Mixing Ratio

Common parameters to describe the stratospheric aerosol size distribution are the aerosol mixing ratios $N_{0.15}$ and $N_{0.25}$, where N_r is the number of particles with radius larger than r in microns, and the aerosol size ratio $N_{0.15}/N_{0.25}$ [*Russell et al.*, 1981]. These parameters are deduced from in situ measurements of stratospheric aerosol with balloon-borne OPC instruments. In Figure 13 a meridional cross section of the simulated aerosol mixing ratio $N_{0.15}$ for the Northern Hemisphere is compared with observations by *Hofmann and Rosen* [1981] made during the nonvolcanic period of 1978-1979. *Hofmann and Rosen* [1981] derived the geographical distribution in the Northern Hemisphere from four different measurement sites (Greenland (67°N), Laramie, Wyoming (41°N), Texas (32°N), and Brazil (2°S)). In contrast to the Laramie data, where a continuous time series exists, the data from the other locations origi-
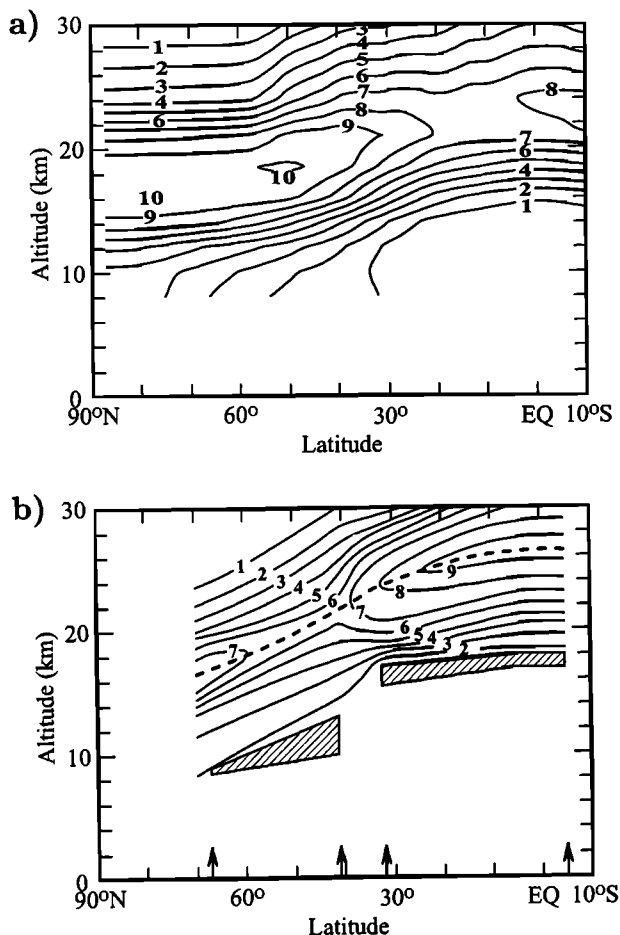
Figure 13. Latitude-altitude cross section of the aerosol mixing ratio $N_{0.15}$, where $N_{0.15}$ is the number of particles with radius > 0.15 μm in unit particles per milligram of air (a) model results (5 year average) and (b) observations for the year 1978 and 1979 by *Hofmann and Rosen* [1981].

nate only from a small number of soundings. In general, the model is able to represent the observed pattern, with maximal values between 8 and 10 particles per milligram air in the lower stratosphere. Local maxima are simulated at the pole and in the tropics, whereby the polar maximum is located at $\sim$ 16 km and the tropical one is located at 20 km.

In comparison to the OPC measurements the calculated tropical maximum concentration (eight particles per milligram) is lower than the observation (nine particles per milligram), while the calculated polar maximum (10 particles per milligram) is higher than the observation (seven particles per milligram). Furthermore, the altitude of the tropical maximum is located $\sim$ 5 km lower in the simulation than in the observation. A possible reason for this difference is the too strong meridional transport of the model. Owing to the unresolved upper branch of the Brewer Dobson circulation the tropical aerosol is preferably transported poleward instead of upward. This clearly shows the limitations of this simulation.

3.8. Effective Radius and Aerosol Mass

Figure 14 represents a meridional cross section of the zonally averaged effective radius. The latitude-altitude cross section of the effective radius reflects the main features of the aerosol mixing ratio cross section in Figure 13. Local maxima of the effective radius can be found at high latitudes where large mass mixing ratio are also predicted. However, in the tropics where high mass mixing ratios are also found, the effective radius does not reach a maximum. The difference might be explained by the fact that a large effective radius corresponds to a large fraction of large particles. The tropics are the source of freshly nucleated particles (Figure 5), and they are also the place where tropospheric particles could reach the upper troposphere/lower stratosphere region because of large-scale transport and deep convection. These processes provide a substantial fraction of particles with radii < 0.15 μm. At middle and higher latitudes, mainly aged sulfate particles are found, which have grown through condensation and coagulation processes.

The simulated effective radii for stratospheric background aerosol have values between 0.1 and 0.2 μm within the observed range of 0.17 μm $\pm$ 0.07μm [*Russell et al.*, 1996]. A comparison with the midlatitude values of previous stratospheric data intercomparisons [*Kent et al.*, 1995] in Table 4 also confirms the good agreement with the observations. The simulated effective radii with values $\sim$ 0.16 μm are $\sim$ 20% higher than the SAGE II data but are still smaller than the passive cavity aerosol spectrometer measurements of 0.25 μm by *Wilson et al.* [1993] and the OPC measurements of 0.26 μm by *Hofmann* [1990]. The large spread of the measurements shows not only the level of observational uncertainty but also the interannual variability of the stratospheric background aerosol. Overall, the simulated effective radii agree quite well with the observations.
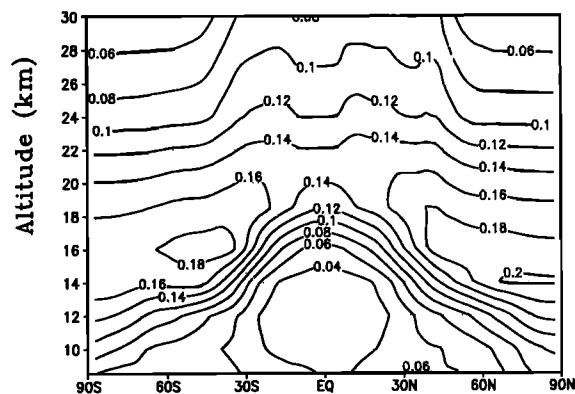

Figure 14. Latitude-altitude cross section of the calculated zonally averaged effective radius (microns).

Table 4. Effective radius

Time	Location	Stratospheric Data Intercomparison (μm)	GCM Results (μm)
1989	41°N; 18-to 22km altitude	0.26 OPC[a]; 0.13 SAGE II[b]	0.14-0.18
Dec. 1988	411°N; 19 km altitude,	0.25 PCS[c]; 0.14 SAGE II[b]	0.16
Spring 1991	41°N; 17-to 21 km altitude	0.11-0.13 OPC[d]; 0.14 SAGE II[b]	0.16-0.19

[a] [*Hofmann*, 1990].
[b] [*Kent et al.*, 1995].
[c] [*Wilson et al.*, 1993].
[d] [*Deshler et al.*, 1993].

3.9. Surface Area Density

The aerosol surface area density is an essential parameter to assess the importance of heterogeneous chemistry processes. Figure 15 shows a comparison between the simulated zonal mean surface area density latitude-height cross sections (5 year average) and surface area densities which are derived from SAGE observations. In Figure 15a the SAGE II seasonal mean of the winter 1988/1989 surface area density [*Thomason et al.*, 1997b] is shown. The stratospheric aerosol load was relatively undisturbed in 1989-1991 though the values were about 10% to 30% higher than observed in 1979

[*Thomason et al.*, 1997a]. Figure 15b shows the surface area density derived from SAGE II, which is recommended by the World Meteorological Organization (WMO) [*World Meteorological Organization*, 1992] for heterogeneous chemistry models. Figure 15c reveals the simulated zonal mean surface area densities as the sum of the size bins with radius $r > 0.001$ μm and in Figure 15d the sum of the size bins with radius $r > 0.1$ μm is shown.

At Northern Hemisphere midlatitudes the model results for $r > 0.001$ μm agree reasonably well with the SAGE data with values of 1.4 μm^2 cm^{-3} at 16 km and
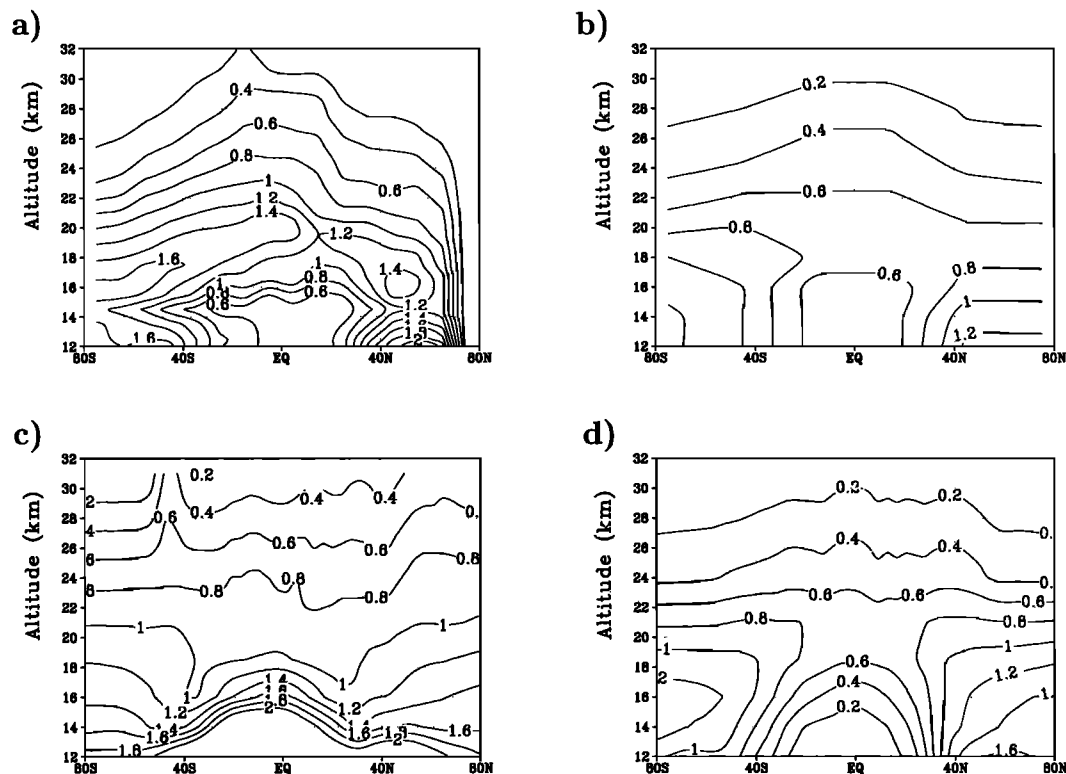

Figure 15. Latitude-altitude cross section of the aerosol surface area density (μm^2 cm^{-3}) (a) aerosol surface area derived from SAGE II data for the year 1988/1989 [*Thomason et al.*, 1997b], (b) aerosol surface area recommended by the World Meteorological Organization [1992], (c) simulated aerosol surface area (5 year average) for $r > 0.001$ μm), and (d) simulated aerosol surface area (5 year average) for $r > 0.1$ μm).

of 1 μm^2 cm^{-3} at 20 km. In the upper tropical tro-posphere, however, the simulated values are about a factor of 2-3 higher than the satellite data. In general, the simulated surface area densities for $r > 0.001$ μm have a quite different geographical distribution than the ones derived from satellite observations. It seems that the surface area density distribution is dominated by a large number of small particles (see Figures 11 and 14). If only aerosol particles with $r > 0.1$ μm are taken into account the simulated surface area density distribution agrees quite well with the observations. Differences be-tween the simulated surface area density distribution for $r > 0.001$ μm and for $r > 0.1$ μm which indicate a large number of small particles, appear in particular in the tropical upper troposphere. The tropical upper tro-pospheric enhancement of small particles is also shown in Figure 14, with very small values of the effective ra-dius below 0.1 μm, which seems to be caused mainly by homogeneous nucleation (Figure 4).

There are some possible reasons for the enhanced amount of small particles in the model simulation in comparison to the observations. One reason might be that the model overestimates the small particles be-cause of the coupling of the microphysical model and the tropospheric sulfur scheme. One indication for this could be the occurrence of great surface area densities in the region of anthropogenic SO$_2$ emissions. Right now the sulfate aerosol is considered in the troposphere with a bulk approach. That means sulfate produced in lower levels is equally distributed to all size classes when an air parcel enters higher levels where aerosol micro-physics is taken into account. Hence the modification of the aerosol size distribution by cloud processing in the troposphere leads not to a shift in the size distribu-tion from smaller to larger particles, as in reality, but to an enhancement of the particle number density in each class. One of the major tasks in the future is therefore the extension of the microphysical stratospheric aerosol model to the troposphere. The shift of the upper tro-pospheric tropical maximum of the homogeneous nucle-ation in the model to the lower stratosphere (Figures 4 and 5) might also lead to an overestimation of small particles in the stratosphere.

Another possible reason for the difference between model simulation and satellite observation may be the fact that SAGE II extinction measurements with the smallest detection wavelength at 0.385 μm give little information about particles smaller than 0.1 μm [Wang et al., 1989; Thomason and Osborne, 1992] and there-fore probably underestimate small particles. In addition to this the uncertainties are in the range ± 30% for a surface area density of 0.1 μm^2 cm^{-3} and ±15% for one of 10 μm^2 cm^{-3} [Thomason et al., 1997b].

It seems therefore appropriate to compare the simu-lated surface area density for $r > 0.1$ μm with the obser-vation. The simulated surface area density distribution is in good agreement with the WMO distribution indi-cating a tropical maximum of 0.6 μm^2 cm^{-3} between
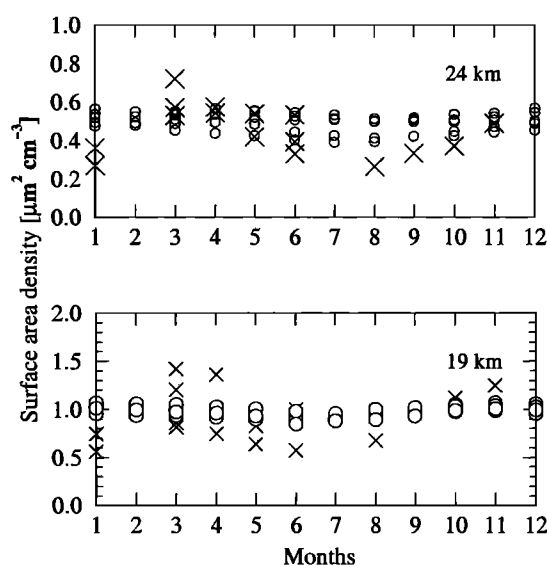

Figure 16. Comparison of the observed aerosol sur-face area density (μm^2 cm^{-3}) at 41°N [T. Deshler, personal communication, 1999] at two different heights with simulated monthly mean values for the correspond-ing grid. The crosses indicate the measurements taken at individual days in the first half of 1991 and between 1996 and 1999 and the circles indicate the simulated monthly mean values for the 5 years.

18 and 20 km and values of 0.4 μm^2 cm^{-3} at 26 km and of 0.2 μm^2 cm^{-3} at 30 km. Differences between model results and WMO data occur in high latitudes of both hemispheres. In the Southern Hemisphere the simulated local maximum of 1.2 μm^2 cm^{-3} is located between 17 km and 13 km, 2 km higher than in the WMO data. In the Northern Hemisphere the simulated values below 24 km are $\sim$ 40% higher in comparison to the WMO distribution.

A relatively good agreement between GCM results and observations is also evident if we compare our sim-ulations with in situ measurements. The monthly av-eraged simulated surface area density for particles with $r > 0.1$ μm at 41°N in comparison to OPC measure-ments from Laramie (T. Deshler, personal communi-cation, 1999) is shown in Figure 16 for two different altitudes (19 km and 24 km).

In general, the GCM results match the observations quite well at all altitudes. Differences between model results and observations, however, occur at certain al-titudes and for certain months. In January and Au-gust the model results are $\sim$ 30% higher at 19 km and at 24 km, while in November at 19 km they are $\sim$ 20% lower. Furthermore, the observations show a considerably larger interannual and monthly variabil-ity. At 19 km the OPC data range between 0.56 and 1.42 μm^2 cm^{-3}, whereas the model results range be-tween 0.86 and 1.1 μm^2 cm^{-3}. A similar behavior can be found at 24 km, where the model results vary be-tween 0.39 and 0.56 μm^2 cm^{-3} and the OPC data vary between 0.26 and 0.72 μm^2 cm^{-3}. A possible reason

for this might be the fact that the OPC data reflect particular days under specific synoptic situations, while the model results represent monthly averages for the simulated years. Furthermore, in the simulations interannual and daily fluctuations in the anthropogenic and volcanic sulfur emission are neglected. In the model, constant monthly mean sulfur sources are used throughout the simulation. The model results could therefore reflect only the atmospheric variability. Hence daily variations in anthropogenic or natural emissions have no impact on our model results. However, the role which anthropogenic sulfur emissions play for the stratospheric aerosol load is still uncertain. Right now SAM is being coupled to a chemistry model CHEM [*Steil et al.*, 1998]. This chemical-microphysical climate model will be a good tool to address this open problem in the near future.

4. Summary and Discussion

The coupling of a microphysical stratospheric aerosol model with a tropospheric sulfur cycle is an important step toward a coupled chemical-microphysical climate model. Results of a first 3-D multiannual background simulation show that the concentration of aerosol precursor gases, SO_2 and $H_2SO_4(g)$, agrees well with in situ measurements. The $H_2SO_4(g)$ concentrations differ up to 1 order of magnitude dependent on the choice of the sticking coefficient α, whereas aerosol properties such as the aerosol mass density are not influenced by α. The best agreement is achieved for $\alpha = 1$.

The formation of new particles through homogeneous nucleation is mainly determined by the temperature and takes place mainly in the tropics and in polar spring in good agreement with aircraft measurements. Owing to the temperature bias in the model's tropical tropopause the homogeneous nucleation maximum is shifted from the upper troposphere to the lower stratosphere. The model results show a distinct interannual and interseasonal variability at all heights with a springtime cleansing at polar latitudes. At northern hemisphere midlatitudes a clear annual cycle with a maximum in winter and a minimum in summer is evident in the aerosol mass concentration at 16 km and to a lesser extent at higher altitudes This interannual variability is the result of stronger downward and poleward transport in the winter hemisphere.

The 3-D simulations reproduce important features of the stratospheric sulfuric acid aerosol. The effective radius and the aerosol mass density correspond well with satellite and in situ measurements for the Northern Hemisphere midlatitude between 1988 and 1991. The model is furthermore able to reproduce the observed vertical distribution of the aerosol mixing ratio in the Northern Hemisphere, but the tropical maximum has a lower and the polar maximum has a higher value compared to the observations. Owing to the inadequately resolved upper branch of the Brewer Dobson

circulation (model top at 10 hPa), the tropical aerosol is preferably transported in the lower transport regime, although both transport regimes exist in the model. The tropical aerosol reservoir is evident in the two uppermost model layers. Aerosol transport from the tropics to the high latitudes occurs in these layers in synoptic-scale tongues in the winter months but also in August. A detailed analysis of the link between the spatial and temporal aerosol distribution and the stratospheric circulation is, however, not possible with the model version used. Owing to the model's upper boundary at 10 hPa the interpretation of the model results is limited. It is therefore planned to repeat the simulations with a middle atmosphere version of the ECHAM model to study the link between aerosol distribution and atmospheric dynamics in more detail.

The simulated aerosol size distributions show a distinct bimodal structure with a shift to smaller radii with altitude. They are in good agreement with in situ measurements at Northern Hemisphere midlatitudes although the model tends to underpredict the amount of very large particles and to overpredict the number of very small particles in comparison to the observations. The simulated aerosol surface area density agrees quite well with values derived from satellite observations and OPC measurements if only aerosol particles with radius $r > 0.1$ μm are taken into account.

In general, SAM seems to overestimate the number of small particles in comparison to the observations. A possible reason for this discrepancy could be the separate treatment of tropospheric sulfate aerosol mass $(m(t))$ and stratospheric sulfate aerosol mass $(m(r,t))$. The coupling between the microphysical model and the sulfur cycle is certainly one of the most critical points of these simulations. The switch between the size resolved approach in the upper nine layers of the model and the bulk approach in the ten tropospheric layers includes a large potential of possible errors. However, owing to this approximation it was possible to simulate realistic global fields of stratospheric sulfuric acid background aerosol, within a limited amount of computing time.

As a next step, it is intended to merge the microphysical model with the tropospheric sulfur scheme in order to calculate global fields of the sulfate aerosol distribution $m(r,t)$ from the surface to the top of the atmosphere. In particular, the following model improvements are planned: (1) Nucleation and condensation parameterizations of the stratospheric model will be extended to tropospheric conditions; (2) the particle formation in clouds, scavenging and deposition processes will be reformulated to account for particle radius; and (3) sulfuric acid gas and carbonyl sulfide will be introduced as prognostic variables. The improved model version will be used to assess the climate impact of a variable stratospheric aerosol concentration and to determine which processes sustain the stratospheric aerosol layer.

References

Arnold, F., and T. Bührke, New H_2SO_4 and HSO_3 vapour measurements in the stratosphere–evidence for a volcanic influence, *Nature*, *301*, 294–295, 1983.

Arnold, F., J. Curtius, S. Spreng, and T. Deshler, Stratospheric aerosol sulfuric acid: First direct in situ measurements using a novel balloon–based mass spectrometer apparatus, *J. Atmos. Chem.*, *30*, 3–10, 1998.

Bates, T. S., D. Cline, R. H. Gammon, and S. R. Kelly-Hansen, Regional and seasonal variations in the flux of oceanic dimethylsulfide to the atmosphere, *J. Geophys. Res.*, *92*, 2930–2938, 1987.

Bekki, S., and J. A. Pyle, Two–dimensional assessment of the impact of aircraft sulphur emissions on the stratospheric sulphate aerosol layer, *J. Geophys. Res.*, *97*, 15,839–15,847, 1992.

Bekki, S., and J. A. Pyle, Potential impact of combined NO_x and SO_x emissions from future high–speed civil transport aircraft on stratospheric aerosols and ozone, *Geophys. Res. Lett.*, , *20*, 723–726, 1993.

Bekki, S., and J. A. Pyle, A two–dimensional modeling study of the volcanic eruption of Mount Pinatubo, *J. Geophys. Res.*, *99*, 18,861–18,869, 1994.

Benkovitz, C. M., C. M. Berkowitz, R. C. Easter, S. Nemesure, R. Wagener, and S. Schwartz, Sulfate over the north Atlantic and adjacent continental regions: Evaluation for October and November 1986 using a three–dimensional model driven by observation–derived meteorology, *J. Geophys. Res.*, *99* 20,725–20,756, 1994.

Berge, E., Coupling of wet scavenging of sulphur to clouds in a numerical weather prediction model, *Tellus, Ser. 45 B*, 1–22, 1993.

Brock, C. A., J. C. Wilson, H. H. Jonsson, and K. R. Chan, Particle formation in the upper tropical troposphere: a source of nuclei for the stratospheric aerosol, *Science*, 270, 1650–1653, 1995.

Chen, P., J. R. Holton, A. O Neill, and R. Swinbank, Isentropic mass exchange between the tropics and the extratropics in the stratosphere, *J. Atmos. Sci.*, *51*, 3006–3018, 1994.

Chlond, A., Locally modified Bott-scheme for highly convective flows, *Mon. Weather Rev.*, *122*, 113–125, 1994.

Clement, C. F., M. Kulmala, and T. Vesala, Theoretical considerations on sticking propabilites, *J. Aerosol Sci.*, *27*, 869–882, 1996.

Curtius, J., B. Sierau and F. Arnold, Airborne measurements of aerosol sulfuric and aerosol precursor gases in the free troposphere during FREETROPE/ACE 2, paper presented at Joint International Symposium on Global Atmospheric Chemistry, CACGP/IGAC, Seattle, Wash., 1998.

Danilin, M. Y., et al., Aviation fuel tracer simulation: Model intercomparison and implications, *Geophys. Res. Lett.*, *25*, 3947–3950, 1998.

Deshler, T., D. J. Hofmann, B. J. Johnson, and W. R. Rozier, Balloon–borne measurements of the Pinatubo aerosol size distribution and volatility at Laramie, Wyoming, during the summer of 1991, *Geophys. Res. Lett.*, *19*, 199–203, 1992.

Deshler, T., B. J. Johnson, and W. R. Rozier, Balloon–borne measurements of Pinatubo aerosol during 1991 and 1992 at 41° N: Vertical profiles, size distribution, and volatility, *Geophys. Res. Lett.*, *20*, 1435–1438, 1993.

Dutton, E. G., and J. R. Christy, Solar radiative forcing at selected locations and evidence for global lower tropospheric cooling following the eruptions of El Chichón and Pinatubo, *Geophys. Res. Lett.*, *19*, 2313–2316, 1992.

Feichter, J., E. Kjellström, H. Rodhe, F. Dentener, J. Lelieveld, and G.-J. Roelofs, Simulation of the tropospheric sulfur cycle in a global climate model, *Atmos. Environ.*, *30*, 1693–1707, 1996.

Fuchs, N. A., Observation of the aerosol layer at 20 km by optical radar. *J. Atmos. Sci.*, *21*, 323–324, 1964.

Ganzeveld, L., J. Lelieveld, and G.-J. Roelofs, A dry deposition parameterization for sulfur oxides in a chemistry and general circulation model, *J. Geophys. Res.*, *103*, 5679–5694, 1998.

Giorgi, F., and W. L. Chameides, Rainout lifetimes of highly soluble aerosols and gases as inferred from simulations with a general circulation model, *J. Geophys. Res.*, *91*, 14,367–14376,1986.

Grant, W. B., et al., Aerosol–associated changes in tropical stratospheric ozone following the eruption of Mount Pinatubo, *J. Geophys. Res.*, *99*, 8197–8211, 1994.

Grant, W. B., E. V. Browell, C. S Long, L. L Stowe, R. G Grainger and A. Lambert, Use of volcanic aerosols to study the tropical stratospheric reservoir, *J. Geophys. Res.*, *101*, 3973–3988, 1996.

Graf, H.-F., J. Feichter and B. Langmann, Volcanic sulfur emissions: Estimates of source strength and its contribution to the global sulfate distribution, *J. Geophys. Res.*, *102*, 10,727-10,738, 1997.

Grooß, J. U., C. Brühl, and T. Peter, Impact of aircraft emissions on tropospheric and stratospheric ozone, Part I: Chemistry and 2-D model results, *Atmos. Environ.*, *32*, 3173–3184, 1998.

Hamill, P., E. J. Jensen, P. B. Russell, and J. J. Bauman, The life cycle of stratospheric aerosol particles, *Bull. Am. Meteorol. Soc.*, *78*, 1395–1410, 1997.

Hao, W. M., M. H. Liu, and P. J. Crutzen, Estimates of annual and regional releases of CO_2 and other trace gases to the atmosphere from fires in the tropics, based on the FAO statistics for the period 1975–1980, in *Fire in the Tropical Biota*, edited by J. G. Goldhammer, pp. 440–462, Springer–Verlag, New York, 1990.

Harvey, V. L., M. H. Hitchmann, R. B. Pierce, and T. D. Fairlie, Tropical aerosol in the Aleutian High, *J. Geophys. Res.*, *104*, 20,689–20,700, 1999.

Haynes, P. E., and M. E. McIntyre, On the evolution of vorticity and potential vorticity in the presence of diabatic heating, *J. Atmos. Sci.*, *44*, 828–841, 1987.

Herman, J. R., and D. Larko, Low ozone amounts during 1992–1993, *J. Geophys. Res.*, *99*, 3483–3496, 1994.

Hitchman, M. H., M. McKay and C. R. Trepte, A climatology of stratospheric aerosol, *J. Geophys. Res.*, *99*, 20,689–20,700, 1994.

Hofmann, D. J., Increase in the stratospheric background sulfuric acid aerosol mass in the past 10 years, *Science*, *248*, 996–1000, 1990.

Hofmann, D. J., and J. M. Rosen, On the background stratospheric aerosol layer, *J. Atmos. Sci.*, *38*, 168–181, 1981.

Hofmann, D. J., and S. Solomon, Ozone destruction through heterogeneous chemistry following the eruption of El Chichón, *J. Geophys. Res.*, *94*, 5029–5041, 1989.

Inn, Y. E., C. J. F. Vedder, and D. O Hara, Measurement of stratospheric sulfur constitutents, *Geophys. Res. Lett.*, *8*, 5-8, 1981.

Kärcher, B., Physiochemistry of aircraft-generated liquid

aerosols, soot, and ice particles, 1. Model description, *J. Geophys. Res., 103,* 17,111–17,128, 1998.

Kent, G. S., C.-R. Trepte, U. O. Farukh and M. P. McCormick, Variation in the stratospheric aerosol associated with the north polar vortex as measured by the sam ii satellite sensor, *J. Atmos. Sci., 42,* 1536-1551, 1985.

Kent, G. S., P.-H. Wang, M. P. McCormick, and K. M. Skeens, Multiyear Stratospheric Aerosol and Gas Experiment II measurments of upper tropospheric aerosol characteristics, *J. Geophys. Res., 100,* 13,875-13,899, 1995.

Kritz, M. A., Formation mechanism of the stratospheric aerosol, Ph.D. thesis, Yale Uni., New Haven, Conn., 1975.

Labitzke, K., and M. P. McCormick, Stratospheric temperature increases due to Pinatubo aerosols, *Geophys. Res. Lett., 19,* 207–210, 1992.

Lacis, A., J. Hansen, and M. Sato, Climate forcing by stratospheric aerosols, *Geophys. Res. Lett., 19,* 1607–1610, 1992.

Meixner, F. X., The vertical sulfur dioxide distribution at the tropopause level, *J. Atmos. Chem., 2,* 175–189, 1984.

Möhler, O., and F. Arnold, Gaseous sulfuric acid and sulfur dioxide measurements in the arctic troposphere and lower stratosphere: Implications for hydroxyl radical abundances, *Geophys. Res. Lett., 19,* 1763–1766, 1992.

Ockelmann, G. E. F., and H. W. Georgii, Grossräumige Verteilung des atmosphärischen Schwefeldioxids in der freien Troposphäre, *Meteorol. Rundsch., 41,* 136-146, 1989.

Pitari, G. and E. Mancini, Stratospheric sulfate aerosols in volcanically quiet conditions in Proceed. of the European workshop on aviation, aerosols, contrails and cirrus clouds (A2C3) edited by U. Schumann and G. T. Amanatidis, pp. 27-32, *Air Pollution Research Report Nr. 74,* Commission of the European Communities, Luxembourg, 2001.

Pitari, G., V. Rizzi, L. Ricciardulli, and G. Visconti, High-speed civil transport impact: Role of sulfate, nitric acid trihydrate, and ice aerosols studied with a two-dimensional model including aerosol physics, *J. Geophys. Res., 98,* 23,141–23,164, 1993.

Pitari, G., E. Mancini, V. Rizi, and D. T. Shindell, Impact of future climate and emission changes on stratospheric aerosols and ozone, *J. Atmos. Sci.,* in press, 2001

Randel, W. J., F. Wu, J. M. Russell III, J. W. Waters, and L. Froidevaux, Ozone and temperature changes in the stratosphere following the eruption of Mount Pinatubo, *J. Geophys. Res., 100,* 16,753–16,764, 1995.

Roeckner, E., K. Arpe, L. Bengtsson, M. Christoph, M. Claussen, L. Dümenil, M. Esch, M. Giorgetta, U. Schlese, and U. Schulzweida The atmospheric general circulation model ECHAM-4: Model description and simulation of the present-day climate, *Rep. 218,* Max–Planck Inst. für Meteorol., Hamburg, Germany, 1996.

Roelofs, G. J., and J. Lelieveld, Distribution and budget of O_3 in the troposphere calculated with a chemistry general circulation model, *J. Geophys. Res., 100,* 20,983–20,998, 1995.

Russell, P. B., T. J. Swissler, M. P. McCormick, W. P. Chu, J. M. Livingston, and T. J. Pepin, Satellite and correlative measurements of the stratospheric aerosol, I, An optical model for data conversions, *J. Atmos. Sci., 38,* 1279–1294, 1981.

Russell, P. B., et al., Global to microscale evolution of the Pinatubo volcanic aerosol, derived from diverse measurements and analyses, *J. Geophys. Res., 101,* 18,745–18,763, 1996.

Spiro, P. A., D. A. Jacob, and J. A. Logan, Global inventory of sulfur emissions with $1° \times 1°$ resolution, *J. Geophys. Res., 97,* 6023–6036, 1992.

Steil, B., M. Dameris, C. Brühl, P. J. Crutzen, V. Grewe, M. Ponater, and R. Sausen, Development of a chemistry

module for GCMs: First results of a multi–annual integration, *Ann. Geophys., 16,* 205–228, 1998.

Thomason, L. W. and M. T. Osborne, Lidar conversion parameters derived from SAGE II extinction measurements, *Geophys. Res. Lett., 19,* 1655–1658, 1992.

Thomason, L. W. and L. R. Poole, Use of stratospheric aerosol properties as diagnostics of Antarctic vortex processes, *J. Geophys. Res., 98,* 23,003–23,012, 1993.

Thomason, L. W., G. S. Kent, C. R. Trepte, and L. R. Poole, A comparison of the stratospheric aerosol background periods of 1979 and 1989-1991, *J. Geophys. Res., 102,* 3611–3616, 1997a.

Thomason, L. W., L. R. Poole, and T. Deshler, A global climatology of stratospheric aerosol surface area density deduced from Stratospheric Aerosol and Gas Experiment II: 1984-1994, *J. Geophys. Res., 102,* 8967–8976, 1997b.

Tie, X., G. P. Brasseur, B. Briegleb, and C. Grainer, Two-dimensional simulation of Pinatubo aerosol and its effect on stratospheric ozone, *J. Geophys. Res., 99,* 20,545–20,562, 1994.

Timmreck, C., Simulationen zur Bildung und Entwicklung von stratosphärischem Aerosol unter besonderer Berücksichtigung der Pinatuboepisode, Ph.D. thesis, Univ. Hamburg, Germany 1997.

Timmreck C., and H.-F. Graf, A microphysical model to simulate the development of stratospheric aerosol in a GCM, *Meteorol. Z.,* 9,263-282, 2000.

Timmreck, C., H.-F. Graf, and J. Feichter, Simulation of Mt. Pinatubo aerosol with the Hamburg climate model ECHAM4, *Theor. Appl. Climatol. 62,* 85-108, 1999.

Toon, O. B., R. P. Turco, P. Hamill, C. S. Kiang and R. C. Whitten A one-dimensional model describing aerosol formation and evolution in the stratosphere: II. Sensitivity studies and comparison with observations, *J. Atmos. Sci., 36,* 718-736, 1979.

Toon, O. B., R. P. Turco, D. Westphal, R. Malone, and M. S. Liu, A multidimensional model for aerosols: Description of computational analogs', *J. Atmos. Sci., 45,* 2123–2143, 1988.

Trepte, C. R., and M. H. Hitchman, Tropical stratospheric circulation deduced from satellite aerosol data, *Nature, 355,* 626–628, 1992.

Trepte, C. R., R. V. Veiga, and M. P. McCormick, The poleward dispersal of Mount Pinatubo volcanic aerosol, *J. Geophys. Res., 98,* 18,563–18,573, 1993.

Turco, R. P., P. Hamill, O. B. Toon, R. C. Whitten, and C. S. Kiang, A one-dimensional model describing aerosol formation and evolution in the stratosphere, I, Physical processes and computational analogs, *J. Atmos. Sci. 36,* 699-717, 1979.

Turco, R. P., R. C. Whitten, O. B. Toon, E. C. Y. Inn, and P. Hamill, Stratospheric hydroxyl radical concentrations: new limitations suggested by gaseous and particulate sulfur, *J. Geophys. Res., 86,* 1129-1139, 1981.

Van Dingenen, R. and F. Raes, Determination of the condensation accommodation coefficient of sulfuric acid on water–sulfuric acid aerosol, *Aerosol Sci. Technol.,* 15, 93–106, 1991.

Wang, P. H., M. P. McCormick, T. Swissler, M. T. Osborn, W. H. Fuller, and G. K. Yue, Inference of stratospheric aerosol composition and size distribution from SAGE II satellite measurements, *J. Geophys. Res., 94,* 8435–8446, 1989.

Waugh, D. W., Seasonal variation of isentropic transport out of the tropical stratosphere *J. Geophys. Res., 101,* 4007–4023, 1996.

Weisenstein, D. K., M. K. W. Ko, N.-D. Sze, J. M. Rodriguez, Potential impact of SO_2 emissions from strato-

spheric aircraft on ozone *Geophys. Res. Lett.*, *23*, 161–164, 1996.

Weisenstein, D. K., G. K. Yue, M. K. W. Ko, N.-D. Sze, J. M. Rodriguez and C. J. Scott, A two–dimensional model of sulfur species and aerosols, *J. Geophys. Res.*, *102*, 13,019–13,053, 1997.

Weisenstein, D. K., M. K. W. Ko, I. G. Dyominov, G. Pitari, L. Ricciardulli, G. Visconti and S. Bekki, The effects of sulfur emissions from HSCT aircraft: A 2-D model inter-comparison, *J. Geophys. Res.*, *103*, 1527–1547, 1998.

Williamson, D. L. and P. J. Rasch, Two–dimensional semi–Lagrangian transport with shape–preserving interpola-tion, *Mon. Weather Rev.*, *117*, 102–129, 1989.

Wilson J. C., M. Loewenstein, D. W. Fahey, B. Gary, S. D. Smith, K. K. Kelly, G. V. Ferry, and K. R. Chan, Observations of condensation nuclei in the airborne arctic ozone experiment: Implications for new particle formation and polar stratospheric cloud formation, *J. Geophys. Res.*, *94*, 16,437–16,448, 1989.

Wilson, J. C., M. R.Stolzenburg, W. E. Clark, M. Loewen-stein, G V Ferry, K. R Chan and K. K. Kelly, Strato-spheric sulfate aerosol in and near the northern hemi-sphere polar vortex: The morphology of the sulfate layer, multimodal size distributions and the effect of denitrifica-tion. *J. Geophys. Res.*, *97*, 7997-8013, 192.

Wilson J. C., et.al., In situ observations of aerosol and chlo-rine monoxide after the 1991 eruption of Mount Pinatubo: Effect of reactions on sulfate aerosols, *Science*, *261*, 1140–1143, 1993.

World Meteorological Organization, Scientific assessment of ozone depletion: 1991, Global Ozone Research and Mon-itoring Project, WMO Rep., 25, Geneva, Switzerland, 1992.

Zhao, J., Numerical studies of the stratospheric aerosol layer under background and perturbed conditions, Ph.D. thesis, Univ. of Calif., Los Angeles, 1993.

Zhao, J., R. P. Turco, and O. B. Toon, A model simula-tion of Pinatubo volcanic aerosols in the stratosphere, *J. Geophys. Res.*, *100*, 7315–7328, 1995.

Yue, G. K., and A. Deepak, Latitudinal and altitudinal vari-ation of size distribution of stratospheric aerosols inferred from SAGE aerosol extinction coefficient measurements at two wavelengths, *Geophys. Res. Lett.*, *11*, 999–1002, 1984.

Yue, G. K., L. R. Poole, P. H Wang, and E. W. Chiou, Stratospheric aerosol acidity, and refractive index deduced from SAGE II and NMC temperature data. *J. Geophys. Res.*, *99*, 3727–3738, 1994.

C. Timmreck, Max-Planck Institut für Meteorologie, Bundesstr. 55, D-20146 Hamburg, Germany. (timm-reck@dkrz.de)